Revision 1

The mafic component of the lunar crust: Constraints on the crustal abundance of mantle and intrusive rock, and the mineralogy of lunar anorthosites

Sarah T. Crites[1,]*, Paul G. Lucey[1], and G. Jeffrey Taylor[1]

[1] Hawai'i Institute of Geophysics and Planetology, University of Hawai'i at Mānoa, 1680 East West Rd POST 602, Honolulu, HI 96822, USA

*Corresponding author. Tel: +1-808-956-3670. Fax: +1-808-956-6322. Email: scrites@higp.hawaii.edu

ABSTRACT

Most models of early lunar evolution predict that the anorthositic highlands crust is the result of plagioclase flotation on a magma ocean. However, the lunar highlands crust typically contains 4 wt% FeO and so is more mafic than the strict definition of the anorthosites thought to comprise it. We used new Clementine-based mineral maps of the Moon as inputs to a series of mixing models that calculate the abundance and distribution of major highland rock types and shed light on three possible sources of excess mafic material in the lunar highlands: mafic (15 vol% mafic minerals) anorthosites, post-magma ocean igneous activity, and mafic basin ejecta. Mixing models that feature pure anorthosites like the purest anorthosite (PAN) described by Ohtake et al. (2009) and Pieters et al. (2009) are most compatible with the data. They allow us to place an upper limit of 10-20 vol% mantle material that could be mixed with the primary highlands crust. The upper limit on mantle material indicated by the mixing models is significantly lower than the 30-40 vol% mantle material expected from simple geometric calculations of the major lunar basins' excavation cavities based on an excavation cavity depth/diameter ratio of 1/10; this discrepancy allows us to conclude that the excavation cavities of the three largest lunar basins may have been significantly shallower than those of the smaller basins. Our results are consistent with excavation cavity depth/diameter ratios for these largest basins in the range of 0.035 to 0.06, which agrees with previous gravity measurements by Wieczorek and Phillips (1999).

Keywords: lunar highlands; anorthosite; magma ocean; spectroscopy

INTRODUCTION

The magma ocean hypothesis (e.g. Smith et al. 1970; Wood et al. 1970; Warren and Wasson 1977; Warren 1985; Snyder et al. 1992) provides a framework for the story of the Moon's early history: a primary crust of anorthosite making up the lunar highlands formed from floating as a melt differentiated; the nearside maria are the result of relatively recent volcanism (Neal and Taylor 1992). Both samples (e.g. Wood et al. 1970; Korotev et al. 2003; Warren 1990) and remote sensing (e.g. Hawke et al. 2003; Prettyman et al. 2006; Ohtake et al. 2009; Pieters et al. 2009; Cheek et al. 2013) provide strong support for the magma ocean hypothesis. However, the typical lunar highlands surface contains 4-5 wt% FeO (Korotev et al. 2003; Prettyman et al. 2006) or over 15 vol% mafic minerals, and so is more mafic than strictly defined anorthosites (<10 vol% mafic minerals, Stöffler et al. 1980), and much more mafic than the very anorthositic "purest anorthosites" (PAN) detected ubiquitously in craters larger than 30 km by Ohtake et al. (2009), which contain less than 2 vol% mafic minerals. This raises the question of the source of the excess mafic material in the lunar highlands that may not be associated with magma ocean anorthosites.

Samples and remote sensing reveal the complexity of the lunar crust (e.g. James 1980; Ryder and Spudis 1980; Pieters 1986; Tompkins and Pieters 1999; Warren 1990) and attest to the variety of processes that could lead to the observed elevated mafic content of the lunar highlands. We examined three possible explanations for the elevated abundances of mafic material: 1) the lunar anorthosites are inherently more mafic than the strict definition, as suggested by Warren (1990); 2) magma ocean anorthosites are mixed with mafic post-magma ocean igneous intrusions (POI) or extrusive volcanism (Ryder and Spudis, 1980); and 3) mafic lower crust or mantle material was excavated by large-scale basins and is mixed with the anorthositic upper crust (Ryder and Wood, 1977). We used mineral maps derived from Clementine UVVIS spectra and improved through reconciliation with Lunar Prospector neutron and gamma ray spectrometer results by Crites and Lucey (in press) to examine the consistency of various combinations of these non-mutually exclusive scenarios. This allows us to constrain the probable mafic content of lunar magma ocean anorthosites and plausible contributions of igneous activity and mantle contamination to the lunar highland crust.

METHODS

We use a new set of global mineral maps (Crites and Lucey, in press) obtained by reconciling the Clementine-based mineral maps of Lucey (2004) with Lunar Prospector gamma ray spectrometer (GRS) 2°/pixel oxide abundances (Prettyman et al. 2006) to obtain estimates of the distributions of the major highland rock types. Lucey (2004) used radiative transfer modeling combined with Clementine UVVIS spectra of immature locations on the Moon to obtain maps of plagioclase, orthopyroxene, clinopyroxene, olivine, and magnesium number. The maps were interpolated between immature locations to create a continuously gridded global dataset. Crites and Lucey (in press) identified systematic discrepancies between the major oxides derived from these mineral maps and geochemical trends in lunar samples and Lunar Prospector GRS oxides, then reconciled these differences to obtain a new set of mineral maps consistent with GRS oxides and sample trends. These maps included the four major minerals and magnesium number (Mg#) maps modified from Lucey (2004) as well as ilmenite based on the TiO_2 maps of Gillis et al. (2003).

Rock types representing three sources of mafic material

Using assumptions about rock type compositions along with the newly refined mineral abundances, we produced a series of mixing models and assessed the validity of the results to guide our conclusions about the relative importance of the three sources of mafic material to the lunar highlands. The rock types we included in our mixing model were: anorthosite, the major crustal magma ocean product; norite, troctolite, and gabbro or mare basalt, used to represent post-magma ocean igneous intrusive or extrusive volcanism and mare basalt contamination; and dunite and pyroxenite, ultramafic rock types representing the lunar mantle. We used dunite and pyroxenite to represent mantle compositions, but locations where both are present in our model results are also consistent with peridotite.

Most magma ocean models agree that the anorthosite in the lunar highlands crust likely formed by flotation of plagioclase crystals on a dense melt (e.g. Snyder et al. 1992), but the extent to which magma ocean processes isolated plagioclase to the exclusion of mafic minerals in anorthosite is uncertain. Warren (1990) concluded from models of anorthosite flotation on a dense melt that the overall resulting suite of anorthosites should contain approximately 15 vol% mafic silicates. Anorthosites in the sample collection show a wide range of mafic contents ranging from the mafic anorthosite of Warren (1990) to the “purest anorthosite” (PAN, <2 vol%

mafics) of Ohtake et al. (2009), with an average mafic content of 7 vol% (Wieczorek et al. 2006). Spectral measurements by the Kaguya Spectral Profiler and Multiband Imager (Ohtake et al. 2009; Yamamoto et al. 2012) and the Moon Mineralogy Mapper (Pieters et al. 2009) showed that nearly pure exposures of anorthite are common across the lunar surface showing that this variety of anorthosite is not uncommon, and in their study of anorthosites exposed at Orientale, Cheek et al. (2013) found that the Inner Rook Ring was almost entirely dominated by extremely low mafic content anorthosites. More mafic feldspathic material is principally found elsewhere in the basin in locations more susceptible to mixing. The observations of Cheek et al. (2013) strongly suggest that LMO anorthosites, at least in the vast Orientale region, have inherently low mafic contents and the mafic anorthosites suggested by Warren are the exception, not the rule. Despite this, mafic anorthosites do occur in the sample collection, so we explored the effect on our mixing models of varying anorthosite mafic content. In order to cover the full range of solutions, we calculated rock type abundances based on pure anorthite (0 vol% mafics), the PAN of Ohtake et al. (2009) with 2 vol% mafics, anorthosites with the lunar sample-based average 7 vol% mafic component, and the 15 vol% mafic anorthosites of Warren (1990).

In addition to defining the total amount of mafic silicates present in anorthosites, the mixing analysis required assumptions about the relative abundances of the three mafic minerals olivine, orthopyroxene, and clinopyroxene in anorthosites. We calculated the average composition of the lunar samples classified as anorthosites catalogued by Cahill and Lucey (2007) and from this average composition (93.3% plagioclase, 3.6% olivine, 2.1% orthopyroxene, and 0.9% clinopyroxene) we obtained these relative abundances of the minerals: 1:0.6:0.2 ol:opx:cpx. We maintained these relative abundances of mafics when incorporating the mafic minerals into anorthosites regardless of the total mafic content assumed, though it is important to note that the relative abundances of the mafic minerals vary widely across ferroan anorthosite suite samples (Warren, 1990; Cahill and Lucey 2007). An alternate approach was considered which permitted the anorthosite mafic composition to vary in proportion with the mafic minerals present in each pixel, but in order to remain consistent with our definition of the mixed highland rock types described below, and to limit free parameters in the model, we used the average lunar sample anorthosite mafic composition in the final mixing models discussed in this paper.

The mafic minerals olivine, orthopyroxene, and clinopyroxene are present in many mixed highland rock types other than anorthosites. For our analysis we simplified the major mafic-bearing rocks to simple binary mixtures of plagioclase and one of the three major mafic minerals. We categorized the rock types into three groups: post-magma ocean highland igneous rocks (POI rocks: norite, troctolite, gabbro); mantle ultramafics (dunite, pyroxenite); and mare basalt. We used the lunar samples catalogued by Cahill and Lucey (2007) as a guide and averaged the major mineral compositions for all samples in each class. For example, the average of the major mineral composition of sample norites is 47.9% plagioclase, 49.3% orthopyroxene, 0.67% clinopyroxene, and 1.6% olivine. We then simplified each rock type to its two main constituent minerals (for example, norite = plagioclase + orthopyroxene) and obtained the average abundance of the two main constituents relative to each other (for norite, 49% plagioclase and 51% orthopyroxene). In all three cases, the two main constituent minerals made up more than 96% of the average rock composition, so the simplification makes only minor changes to rock composition while significantly decreasing the complexity of the modeling effort. Table 1 shows the simplified rock compositions obtained by this method.

The assignment of clinopyroxene to lunar rock types presents a special complication. The mixed clinopyroxene and plagioclase highland rock type defined by Stöffler et al. (1980) is gabbro, but high-Ca pyroxene is not common in highland rocks samples (James 1980; Taylor et al. 1991). Although recent remote spectral measurements by Ogawa et al. (2011) that suggest that high-Ca pyroxene may be more abundant in the highlands than previously suspected, the dominant clinopyroxene-bearing rock in lunar samples is by far mare basalt (Papike et al. 1998). Furthermore, as a result of the heavy bombardment of the lunar surface, mare basalt fragments are present in nearly all regolith breccia lunar meteorites, including in feldspathic meteorites that may originate from the farside highlands, so at least some mixing of mare rocks with the highlands surface is certain (Korotev et al. 2006). For most of our calculations we therefore assigned clinopyroxene to mare basalt contamination rather than to the POI rock gabbro. We averaged the compositions of mare basalts from Taylor et al. (1991), and, making the assumption that clinopyroxene dominates over orthopyroxene, simplified to plagioclase and clinopyroxene, then calculated the relative abundances of these two minerals. The result of this calculation is shown in Table 1.

In addition to primary magma ocean rocks (anorthosites), post-magma ocean highlands igneous activity (POI rocks, norite, gabbro, and troctolite), and mare basalt contamination, the mafic minerals can by carried by ultramafic mantle rocks. The Moon has experienced a violent bombardment history and several of the largest basins may have penetrated through the lunar crust to excavate mantle material (e.g. Spudis 1993; Lucey et al. 1998; Wieczorek et al. 2013). We simplified the endmember ultramafic rock types defined by Stöffler et al. (1980) to their primary constituents so that dunite was composed entirely of olivine and pyroxenite was composed of orthopyroxene and clinopyroxene in the proportions in which they were present in each pixel. In some runs of the mixing model we excluded clinopyroxene from the mantle in order to assess its effect on our mantle volume estimates; in these cases, pyroxenite consisted entirely of orthopyroxene.

Limits on the volume of mantle excavated

The mineral maps, along with the assumed rock type compositions, allowed us to calculate endmember cases in which all excess mafic minerals not in anorthosites were assigned either to norite, troctolite, and gabbro/mare basalt, or to the mantle ultramafics dunite and pyroxenite. However, the reality likely falls between the endmember cases, with some of the excess mafic material being contributed by large basin ejecta and some contributed by post-magma ocean igneous activity. These intermediate cases required an independent estimate of the relative abundance of crust and mantle. An estimate of the quantity of basin ejecta and percentage of mantle material can be calculated for the known lunar basins and this quantity used as an upper limit for mixing models. We used the geometric model described by Spudis (1993) to calculate the volume of mantle ejected by lunar basins. A number of assumptions including the ratio of the excavation depth to the excavation cavity diameter, the crustal thickness, and the appropriateness of applying proportional scaling to multiring basins affect the estimate of mantle volume excavated, so we performed mixing models using a range of assumptions that resulted in a range of mantle volumes excavated.

Spudis (1993) modeled the ejection cavities of five lunar multiring basins as the intersection of a spherical Moon with a hemispherical cavity penetrating to a depth of one-tenth its diameter based on the model of Croft (1981). The volume of mantle excavated was calculated as the intersection of the hemispherical ejection cavity with a smaller sphere with a radius equal to the difference between the average radius of the Moon and the original crustal thickness at the basin location (Spudis 1993) (that is, a sphere defined by the crust-mantle boundary). We followed the method of Spudis (1993) to calculate the total volume ejected by all 42 multiring basins defined by Spudis (1993) and also included the basin South Pole-Atiken (SPA). Although the lunar surface has been modified by innumerable craters smaller than the 43 basins examined in this study, even the largest of these are expected to excavate from comparatively shallow depth, unless they are located in regions of extremely thin crust, for example within larger basins (e.g. Croft, 1981, Spudis 1993). The numerous smaller impacts would also have contributed to and modified the megaregolith, but at a localized scale as studied by Li and Mustard (2003), so for this global-scale study we focus on the effects of the largest basins.

Following the method of Spudis (1993), the transient crater diameter was used to define the circle of intersection of the sphere of the Moon with the sphere of the excavation cavity. We used transient crater diameter estimates from Table 2 of Petro and Pieters (2004). The excavation cavity depth was obtained by multiplying the diameter of the transient cavity by an excavation cavity depth/diameter ratio. We define the excavation cavity depth/diameter ratio as the ratio of the deepest point from which material is excavated to the transient crater diameter, which is identical to the excavation cavity diameter (Spudis 1993). The excavation cavity depth is significantly shallower than the transient crater depth, which is typically cited as 1/3 the transient crater diameter (e.g. Croft 1980; Spudis 1993). We used an excavation cavity depth/diameter ratio of 0.1 for our initial calculations (e.g. Croft 1980, O'Keefe and Ahrens 1993, Wieczorek and Phillips 1999), and later varied this ratio to obtain mantle volume percentages consistent with our observations. Simple geometry was used to obtain the radius of the sphere that defined the excavation cavity from the transient cavity diameter and the excavation depth, as shown in Figure 1. We calculated the total volume of ejecta and the volume of mantle ejected from all basins in two cases, using average crustal thicknesses of 34 and 43 km from the Gravity Recovery and Interior Laboratory (Wieczorek et al. 2013). Table 2 shows these calculations, which resulted in a total volume of 259 $x10^6$ km^3 excavated by the 43 basins, with 32 vol% (crustal thickness 43 km) to 40 vol% (crustal thickness 34 km) of this made up of mantle material.

The signature of this basin ejecta may have been detected in remote sensing data. Ohtake et al. (2009) found highly anorthositic basement rocks ubiquitously exposed in craters of diameters greater than 30 km in the lunar highlands, indicating that craters larger than 30 km in diameter begin to encounter a pure anorthosite crust, penetrating through a mixed layer that is by inference approximately 3 km thick (Ohtake et al. 2009). The volume of this hypothesized 3 km mixed layer is 116 x 10^6 km^3, roughly consistent with the total volume of ejecta calculated according to the Spudis (1993) method and suggesting that the upper several km of the Moon could be largely composed of basin ejecta and contain several tens of percent mantle material.

These estimates indicate that the upper several km of the Moon's surface could be composed of basin veneer and provide an upper limit on the amount of mantle present in this layer. However, other authors have arrived at lower estimates for the total volume of ejecta from the lunar basins. Petro and Pieters (2008) used two models (Pike 1974 and Housen et al. 1983) to calculate that cumulative basin ejecta from the 41 lunar multiring basins, excluding SPA, covers the Moon to thicknesses between 100 and 1000 m. These thicknesses are equivalent to a total volume of 3.8 to 38 x 10^6 km^3 of basin ejecta, excluding the contribution of SPA. In order to compare directly to our estimates we calculated the contribution of SPA to the total ejecta volume (SPA contributes 55% of the total basin ejecta volume in our estimate based on the method of Spudis (1993)) and added this proportion back in to the ejecta volume calculated from the thicknesses of Petro and Pieters (2008) for a total basin ejecta volume ranging from 5.88 to 58.8 $x10^6$ km^3. These numbers are significantly smaller than those we calculated using the method of Spudis (1993) and are one to two orders of magnitude smaller than the 3 km mixed zone implied by the Ohtake et al. (2009) observations. This allows for the possibility that the upper 3 km zone is not just composed of basin veneer but is instead basin ejecta mixed with a substantial portion of preexisting local crustal material.

To estimate the volume of mantle present in the upper 3 km mixed zone in this low basin ejecta volume case, we scaled our total quantity of basin ejecta to the total basin ejecta volumes from each model used by Petro and Pieters (2008) (5.88 and 58.8 x 10^6 km^3). We scaled our mantle volume ejected (for both 34 and 43 km crustal thickness) by the same factor to obtain a scaled-down total volume of mantle present in the crust if the estimates of Petro and Pieters (2008) better represent the total volume ejected from lunar basins. These values, combined with the total volume of the 3 km mixed zone, result in mantle volume percent in the upper 3 km of 1.67 to 16.7 vol% (43 km crustal thickness) or 2.09 to 20.9 vol% (34 km crustal thickness). Because the differences between the two crustal thickness estimates are much less than the order of magnitude range in ejecta thickness from Petro and Pieters (2008), we simplified the range of mantle volume in the upper mixed zone to between 2 and 20 vol%, both derived from scaling our calculations based on the model of Spudis (1993) to the work of Petro and Pieters (2008).

This wide range of estimates for the contribution of mantle material to the upper mixed zone demonstrates that the question of how much mantle material was excavated by the largest lunar basins is only loosely constrained. We applied each calculated estimate for the volume of mantle excavated (40, 30, 20, and 2 vol%) as upper limits to the mantle ultramafics permitted in each highlands pixel in our mixing models and assessed the plausibility of each result. By assessing how well each estimate for mantle volume excavated agrees with the results of our mixing models, we may be able to place constraints on which models of basin excavation reflect the reality observed by remote sensing.

Rock type distribution calculation

The calculations assigning the major lunar minerals to the rocks made up by these minerals were based around the simplified rock type compositions discussed in the previous sections. The calculations were performed based on a standard procedure and followed different paths depending on assumptions regarding the presence and abundance of mantle ultramafics, the rock type to which clinopyroxene was assigned, and the mafic content of anorthosites. The flowchart of Figure 2 illustrates the method that is described in the following paragraphs, and Table 3 shows the input variables for the different scenarios calculated. 48 possible scenarios exist given these variables; we have calculated rock type abundances for a representative 19 of these scenarios, selected to provide insight into the full range of compositional possibilities but with an emphasis on more realistic scenarios. For example, we calculated two scenarios assuming anorthosites contained no mafic minerals whatsoever (are pure anorthite) in order to assess how this endmember affected the models; however, sample anorthosites contain at least 1% mafics (Cahill and Lucey 2007), so we focused more attention on models assuming purest anorthosite (2 vol% mafics) and other mixed compositions. The results of all paths calculated along with rock type abundance maps for these scenarios can be found in the supplementary material.

We describe here the process of arriving at rock type abundances through any of the branches of Figure 2. We first selected whether to put any mafics into mantle material for the scenario being calculated. If the given scenario did not include mantle ultramafics as a source of mafic material to the highlands, a system of simultaneous unmixing equations were solved for the abundances of anorthosite, norite, troctolite, and gabbro (or mare basalt). If instead the scenario we chose included a mafic contribution from the mantle, the next step was to determine whether an upper limit would be placed on the total mantle volume permitted. Our mantle volume calculations of the previous section were used as upper limits for the total mantle ultramafic rocks permitted in each pixel; however, we also calculated scenarios in which all excess mafics not in anorthosites were of mantle origin to put an upper limit on the total amount of mantle material the measured mineral distributions could support. If there was no limit on the maximum amount of mantle allowed in a scenario (or path), we next chose whether to permit clinopyroxene in the mantle. The simplest scenarios assigned all three mafic minerals to the mantle in the relative abundances in which they were present in each pixel, allowing us to derive an estimate of mantle composition. However, we also calculated rock abundances assuming clinopyroxene did not originate in the mantle. If clinopyroxene was allowed in the mantle, all plagioclase was assigned to anorthosite, which was completed by adding in the appropriate proportions of the mafics, and the remaining mafics were assigned to dunite and pyroxenite. If clinopyroxene was not permitted in the mantle, simultaneous equations were solved to obtain the abundance of mare basalt and anorthosite, and all excess olivine and orthopyroxene was assigned to dunite and pyroxenite.

If an upper limit on permitted mantle abundance was imposed (2, 20, 30, or 40 vol% from our basin ejecta calculations), the total amount of mafic material needed to assign all plagioclase to anorthosite of the selected mafic content was subtracted from the mafic material available to work with and reserved. The remaining mafic minerals were incorporated into dunite and pyroxenite up to the upper limit selected. Any excess mafics remaining above the upper limit were added back into the mafic material reserved for anorthosites, and these mafic minerals and the plagioclase abundance were then fed into the system of equations to obtain anorthosite, norite, troctolite, and gabbro (or mare basalt) abundance. If in this scenario clinopyroxene was not permitted in the mantle, all clinopyroxene would be reserved, the mantle would be constructed out of olivine and orthopyroxene, and the excess olivine and orthopyroxene would be incorporated into anorthosite, norite, and troctolite, with the clinopyroxene going into anorthosite and mare basalt.

In every branch of the flowchart, when anorthosite abundance was calculated, any pixel lacking enough of any one mafic mineral to complete the anorthosite (for example, if anorthosites are PAN, any pixel with >98 vol% plagioclase) was assigned "no solution," meaning that the assumptions about anorthosite composition were incompatible with the measured mineral abundances at that pixel. We tracked the percentage and distribution of no-solution pixels for each scenario, as well as the limiting mafic mineral for each pixel, and report only compositions obtained from those pixels where solutions were obtained. It is important to note that while some no-solution pixels were the result of plagioclase abundance too high to permit anorthosite of the mafic content assumed (for example, a pixel containing 95% plagioclase when mafic anorthosites containing 15 vol% mafics are assumed), other no-solution pixels were governed by the relative mafic abundances assumed, so that a pixel with 85% plagioclase could return no solution if olivine, orthopyroxene, and clinopyroxene were not present in the assumed proportions. Our assumption, based on lunar sample compositions, of anorthosite mafic proportions of 1:0.6:0.2 ol:opx:cpx means that no-solution pixels are most sensitive to low olivine abundance. We calculated the percentage of highland pixels with no-solution results, which provides a measure of how well each set of assumptions about anorthosite composition agreed with the measured mineral abundances. For the scenarios that included an upper limit on the abundance of mantle material, we calculated percent of pixels in which the mantle abundance fell below the upper limit. This provides a measure of how well each mantle constraint agreed with the measured minerals.

As an example of the calculations, we illustrate the process for a single 2x2 degree pixel in the nearside highlands which consists of 70.2 vol% plagioclase, 16.3 vol% clinopyroxene, 7.6 vol% orthopyroxene, and 4.8 vol% olivine in the mineral maps of Crites and Lucey (in press). In order to convert these minerals to rock abundances for a particular mixing model, we began by making the initial assumptions that anorthosites contain 2 vol% mafic minerals and that some basins could have excavated mantle material, but no more than 2 vol% was excavated. Next we reserved enough mafic minerals to allocate all of the plagioclase in the pixel to anorthosite. In this scenario, we assumed anorthosites contain 2% mafic minerals and 98% plagioclase, and the mafic minerals are present according to a 1:0.6:0.2 ratio of olivine to orthopyroxene to clinopyroxene, so 0.77 vol% olivine, 0.45 vol% orthopyroxene, and 0.2 vol% clinopyroxene were reserved. The remaining olivine and both pyroxenes were assigned to dunite and pyroxenite, respectively, in the proportions in which they are present at that pixel (1:1.77:3.99 ol:opx:cpx) up to a limit of 2 vol% total mantle material. This resulted in 0.33 vol% dunite and 1.66 vol% pyroxenite present at this pixel, and leaving 3.7 vol% excess olivine, 6.62 vol% excess orthopyroxene, and 14.97 vol% excess clinopyroxene. These excess mafics were then added back to the quantities initially reserved to create anorthosite, and a system of simultaneous equations was solved for the abundances of anorthosite, norite, and troctolite given their assumed mineral compositions from Table 1. This resulted in a final model composition of 53.6 vol% anorthosite, 13.2 vol% norite, 8.38 vol% troctolite, 22.7 vol% mare basalt, 0.33 vol% dunite, and 1.67 vol% pyroxenite for the selected pixel.

RESULTS AND DISCUSSION

The global rock abundance maps for the model scenario described in the previous paragraph are shown in Figure 3. For this representative scenario, anorthosites were assumed to contain 2 vol% mafic minerals ("purest anorthosites" of Ohtake et al. 2009) and the mantle component was limited to a maximum of 2 vol% in keeping with the lower of the basin ejecta estimates of Petro and Pieters (2008) based on the model of Housen et al (1983). In this scenario, only 7% of the highlands surface returned a "no solution" result, indicating that the measured mineralogy of the highlands is generally consistent with anorthosites of PAN composition and with our assumptions about the relative proportions of the mafic minerals in anorthosites. The map of Figure 3g) shows the spatial distribution of pixels where our assumptions about anorthosite composition were not in agreement with the mineral maps, as well as the limiting mafic mineral for each pixel (red: orthopyroxene; green: olivine; blue: clinopyroxene). The majority of the "no solution" pixels for this scenario occured in the central farside highlands, which are very plagioclase-rich in the mineral maps of Crites and Lucey (in press). The map of Figure 3g) demonstrates that in most of the pixels with insufficient mafic minerals to create plagioclase with 2 vol% mafics in the proportions we assume, orthopyroxene was the limiting factor, reflecting an orthopyroxene low in the central farside highlands in the maps of Crites and Lucey (in press) that is also apparent in the norite distribution.

The norite distribution (Figure 3b) also shows a high-norite anomaly north of Mare Frigoris that corresponds with the Northern Imbrium Noritic (NIN) region observed by Pieters (2002) and further analyzed by Isaacson and Pieters (2009) and Klima et al. (2011). Figure 3b shows norite abundances as high as 15 vol% in this region, among the highest seen anywhere except within SPA. However, the noritic region observed in our rock abundance maps is more extensive than that defined by Isaacson and Pieters (2009), with high norite occurrences as far east as 35°E. The pyroxenite map of Figure 3f, which is influenced by the distribution of both low-Ca and high-Ca pyroxene, also shows elevated abundances throughout the region north of Mare Frigoris as well as within SPA. The signature of elevated high-Ca pyroxene in SPA is also seen in mare basalt abundances (Figure 3d), which range as high as 50% in some areas of the basin in this scenario.

The results of all scenarios taken together are instructive. In particular, in all scenarios that assumed anorthosites contain 15 vol% mafic minerals, 66% or more of highland pixels encounter no-solution, with three-quarters of pixels encountering no-solution in most cases. This suggests that the mafic anorthosites of Warren (1990) are largely not compatible with the measured mineralogy of the highlands, because in the maps of Crites and Lucey (in press) many highland pixels contain more than 85 vol% plagioclase.

The average anorthosite abundance was relatively consistent across all scenarios, with the major controlling factor being the rock type containing the mafic minerals. When the majority of mafic minerals were assigned to POI rocks, which require plagioclase, anorthosite abundance was between about 55 and 65 vol%. Alternatively, when the majority of mafics were assigned to the mantle, average anorthosite abundance ranged from about 70 to 85 vol%. The total amount of mafic contaminant of the primary magma ocean-derived crust ranged from about 15 vol% if all mafics were in the mantle and anorthosites were mafic, to 45% if all mafics were in post-magma ocean igneous rocks and anorthosites contained little or no mafic material. These results are in good general agreement with the estimate of Warren (1990) that the highlands crust is made up of 45-75% ferroan anorthosite suite rocks, or direct products of the magma ocean, with the rest made up of "Mg-rich" rocks. At present there are few constraints available to differentiate between mantle and igneous rocks for assignment of mafic minerals; however, our basin ejecta calculations provide a starting point for estimating the amount of mafic material that may be assigned to ejected mantle (Figure 4).

In the scenarios allowing up to 30-40 vol% mantle (using the Spudis 1993 basin excavation model), from 60 to over 90% of pixels contained less than the maximum amount of mantle allowed, indicating that the data do not support such large proportions of mantle material. The simple ejecta volume calculations based on Spudis (1993) therefore appear to overestimate the amount of mantle excavated compared with the mantle content permitted by measured mineralogy, regardless of other factors such as mafic content of anorthosites. A mantle abundance of about 20 vol% appears more consistent with measured mineralogy: about half of the pixels in these scenarios contained less than 20 vol% mantle. The exception is the case where clinopyroxene was not permitted in the mantle: if the mantle were composed only of olivine and orthopyroxene, very few pixels contained more than 20 vol% mantle. A maximum mantle abundance of 2 vol% (imposed by the lesser basin ejecta thickness model in Petro and Pieters, 2008) required a significant amount of POI and mare basalt rocks in addition to mantle material to account for all mafic minerals, regardless of the mafic content of anorthosites. It is likely that reality reflects some version of this scenario, and the mafic contamination of the lunar highlands is a combination of mantle material, post-magma ocean igneous rocks, and mare basalt contamination. We have constrained the maximum likely amount of mantle present to less than 20 vol%, or nearer 10 vol% if clinopyroxene is not present in the mantle. With these constraints in mind, we summarize the most plausible mixing model results in Table 4.

The percent of mantle material most consistent with the highlands mineralogy is closer to the range of basin ejecta volume calculations based on the ejecta thicknesses of Petro and Pieters (2008) than to our direct geometrical calculation of ejecta volume based on the model of Spudis (1993) chiefly because the latter model emplaces more mafic mantle material than most of the mineral maps can support. A way of reconciling the two estimates is to adjust the depth/diameter ratio of the excavation cavity used in the geometrical ejecta volume calculation. The excavation cavity depth/diameter ratio of 1/10 used by Spudis (1993) appears to be strongly supported for the smaller multiring basins (e.g. Croft 1980, O'Keefe and Ahrens 1993, Wieczorek and Phillips 1999), though a recent study of crater rim constituents using Lunar Reconnaissance Orbiter Camera data by Sharpton (2014) calls this fundamental assumption into question and suggests that the excavation cavity depth/diameter ratio for all lunar craters may be closer to 0.03 or even shallower. Wieczorek and Phillips (1999) found that for the three largest lunar basins SPA, Imbrium, and Serenitatis, the excavation cavity is significantly shallower than 1/10 based on gravity measurements: the excavation cavity depth/diameter ratio for Serenitatis and Imbrium was found to be near 0.05; for SPA it was near 0.01. As 70% of the total ejecta volume and over 90% of the mantle volume in our calculations was from these three largest basins, the smaller excavation cavity depth/diameter ratio suggested by Wieczorek and Phillips (1999) would have a significant effect on the total volume of mantle expected. Depth/diameter ratios of 0.035 to 0.06 for the excavation cavities of the basins resulted in a range of 2 to 23 vol%

mantle in the surface we mapped, and are in better agreement with the mafic mineral abundances mapped than the originally calculated 30-40 vol%.

IMPLICATIONS FOR LUNAR CRUST FORMATION

Our mixing models built from Clementine-based, Lunar Prospector-validated mineral maps allow us to shed light on three possible sources of excess mafic material in the lunar highlands. The maps of Crites and Lucey (in press) indicate a plagioclase-rich crust and across much of the highlands our mixing models are more compatible with a magma ocean that produced the pure anorthosites (<2 vol% mafics) detected widely by spectroscopic methods (e.g. Ohtake et al. 2009; Pieters et al. 2009; Cheek et al. 2013) rather than the mafic anorthosites (15 vol% mafics) suggested by Warren (1990). About 20% of the highlands surface is incompatible with anorthosites containing the intermediate 7 vol% mafics seen on average in lunar samples indicating that although most of the primary anorthosite crust could contain 7 vol% mafics, a significant portion still requires anorthosites of higher purity.

Simple geometric calculations of the amount of mantle that could have been excavated by the lunar multiring basins permit all of the mafic highland material to be derived from mantle ultramafics. However, the assumption about the nature of high-Ca pyroxene has a large impact on the model abundance of mantle. When high-Ca pyroxene was attributed to mare basalt contamination rather than mantle material, nearly 20 vol% mare basalt material was required in the lunar highlands, and only 10 vol% excavated mantle contaminant was present in the crust. This low mantle abundance implies that the excavation cavity depth/diameter ratio for at least the largest lunar basins must be in the range of 0.035 to 0.06, a result consistent with the observation of Wieczorek and Phillips that Serenitatis, Imbrium, and SPA do not have excavation cavity depth/diameter ratios of 1/10. This result could also be explained by a new model of lunar crater excavation described by Sharpton (2014), which indicates that all craters and basins should have excavation cavities with depth/diameter ratios closer to 0.03. These conclusions including the high mare basalt abundance are the result of high clinopyroxene abundance in the maps of Crites and Lucey (in press). Lucey et al. (2014) report very little high-Ca pyroxene in the lunar highlands, which would eliminate the need for extensive mare basalt contamination in the highlands.

Our mixing models allow us to bracket the average mafic contamination of the primary anorthosite crust to between 15 vol% (if the mafic contamination is entirely composed of ultramafic mantle ejecta) and 45 vol% (if the mafic contamination is a result of post-magma ocean igneous activity producing troctolites, norites, and gabbros or mare basalt). Figure 4 shows the field of mafic contaminant sources consistent with our mineral maps. While mineral abundances permit us to put an upper limit of 10-20 vol% on the amount of mantle material that could reasonably be present in the lunar highlands, additional constraints are needed to determine whether a lower limit can be placed on the mantle contribution (that is, whether any mantle material was excavated) so that the relative contributions of mantle vs. post-magma ocean igneous material can be better understood.

REFERENCES CITED

Cahill, J.T. and Lucey, P.G. (2007) Radiative transfer modeling of lunar highland spectral classes and relationship to lunar samples. Journal of Geophysical Research, 112, E10007.

Cheek, L.C., Donaldson Hanna, K.L., Pieters, C.M., Head, J.W., and Whitten J.L. (2013) The distribution and purity of anorthosites across the Orientale basin: New perspectives from Moon Mineralogy Mapper data. Journal of Geophysical Research, 118, doi: 10.1002/jgre.20126.

Crites, S.T. and Lucey, P.G. (in press) Revised mineral and Mg# maps of the Moon from integrating results from the Lunar Prospector neutron and gamma ray spectrometers with Clementine spectroscopy. American Mineralogist, doi: 10.2138/am.2014.4874.

Croft, S.K. (1980) Cratering flow fields: Implications for the excavation and transient expansion stage of crater formation. Proceedings of the 11th Lunar and Planetary Science Conference, p. 2347-2378.

Croft, S.K. (1981) The excavation stage of basin formation: A qualitative model. In Merrill, R.B. and Schultz, P.H., Eds., Proceedings of the Conference on Multi-Ring Basins: Formation and Evolution, pp 207-225, Pergamon, New York.

Gillis, J.J., Jolliff, B.L., and Elphic, R.C. (2003) A revised algorithm for calculating TiO2 from Clementine UVVIS data: A synthesis of rock, soil, and remotely sensed TiO2 concentrations. Journal of Geophysical Research, 108, E2, 5009, doi: 10.1029/2001JE001515.

Hawke, B.R., Peterson, C.A., Blewett, D.T., Bussey, D.B.J., Lucey, P.G., Taylor, G.J., and Spudis, P.D. (2003) Distribution and modes of occurrence of lunar anorthosite. Journal of Geophysical Research, 108, E6, 5050, doi: 10.1029/2002JE001890.

Housen, K.R., Schmidt, R.S., and Hoslapple, K.A. (1983) Crater ejecta scaling laws: Fundamental forms based on dimensional analysis. Journal of Geophysical Research, 88, 2485-2499.

Isaacson, P.J. and Pieters, C.M. (2009) Northern Imbrium Noritic Anomaly, Journal of Geophysical Research, 114, E09007, doi: 10.1029/2008JE003293.

James, O.B. (1980) Rocks of the early lunar crust. Proceedings of the Lunar and Planetary Science Conference 11^{th}, pp 365-393.

Klima, R.L., Pieters, C.M., Boardman, J.W., Green, R.O., Head, J.W. III, Isaacson, P.J., Mustard, J.F., Nettles, J.W., Petro, N.E., Staid, M.I., Sunshine, J.M., Taylor, L.A., and Tompkins, S. (2011) New insights into lunar petrology: Distribution and composition of prominent low-Ca pyroxene exposures as observed by the Moon Mineralogy Mapper (M^3), Journal of Geophysical Research, 116, E00G06, doi: 10.1029/2010JE003719.

Korotev, R.L., Jolliff, B.L., Ziegler, R.A., Gillis, J.J., and Hasken, L.A. (2003) Feldspathic lunar meteorites and their implications for compositional remote sensing of the lunar surface and the composition of the lunar crust. Geochimica et Cosmochimica Acta, 107, 24,4895-24,4923, doi:10.1016/j.gca.2003.08.001.

Korotev, R.L., Ziegler, R.A., and Jolliff, B.L. (2006) Feldspathic lunar meteorites Pecora Escarpment 02007 and Dhofar 489: Contamination of the surface of the lunar highlands by post-basin impacts. Geochimica et Cosmochimica Acta, 70, 5935-5956, doi:10.1016/j.gca.2006.09.016.

Li, L. and Mustard, J.F. (2003) Highland contamination in lunar mare soils: Improved mapping with multiple end-member spectral mixture analysis (MEMSA), Journal of Geophysical Research, 108, E6, 5053, doi: 10.1029/2002JE001917.

Lucey, P.G. (2004) Mineral maps of the moon. Geophysical Research Letters, 31, L08701, doi:10.1029/2003GL019406.

Lucey, P.G., Norman, J.A., Crites, S.T., Taylor, G.J., Hawke, B.R., Lemelin, M., and Melosh, H.J. (2014) A large spectral survey of small lunar craters: Implications for the composition of the lunar mantle, American Mineralogist, 99, 2251-2257, doi: 10.2138/am-2014-4854.

Lucey, P.G., Taylor, G.J., Hawke, B.R., and Spudis, P.D. (1998) FeO and TiO2 concentrations in the South Pole-Aitken basin: Implications for mantle composition and basin formation. Journal of Geophysical Research, 103, 3701-3708.

NASA/GSFC/Arizona State University, WAC Global Morphologic Map, 16 ppd. Lunar Reconnaissance Orbiter Camera. Web. Accessed 7 Jan. 2013. <lroc.sese.asu.edu>.

Neal, C.R. and Taylor, L.A. (1992) Petrogenesis of mare basalts: A record of lunar volcanism. Geochimica et Cosmochimica Acta, 56, 2177-2211.

O'Keefe, J.D. and Ahrens, T.J. (1993) Planetary cratering mechanics. Journal of Geophysical Research, 98, 17,011-17,028.

Ogawa, Y., et al. (2011) The widespread occurrence of high-calcium pyroxene in bright-ray craters on the Moon and implications for lunar-crust composition. Geophysical Research Letters, 38, L17202, doi: 10.1029/2011GL048569.

Ohtake, M. et al. (2009) The global distribution of pure anorthosite on the Moon. Nature, 461, 236-240.

Papike, J.J., Ryder, G., and Shearer, C.K. (1998) Lunar Samples. In Papike, J.J. Ed., Planetary Materials, Reviews in Mineralogy 36, pp 5-1-5-234, Mineralogical Society of America.

Petro, N.E. and Pieters, C.M. (2004) Surviving the heavy bombardment: Ancient material at the surface of South Pole-Aitken Basin. Journal of Geophysical Research, 109, E06004, doi: 10.1029/2003JE002182.

Petro, N.E. and Pieters, C.M. (2008) The lunar-wide effects of basin ejecta distribution on the early megaregolith. Meteoritics and Planetary Science, 43, 1517-1529.

Pieters, C.M. (1986) Composition of the lunar highland crust from near-infrared spectroscopy. Reviews of Geophysics, 24, 557-578.

Pieters, C.M. (2002) Give and take between SPA and Imbrium basins, 33rd Lunar and Planetary Science Conference, Houston, TX, Abstract #1776.

Pieters, C.M. et al., (2009) Mineralogy of the lunar crust in spatial context: first results from the Moon Mineralogy Mapper (M^3). 40th Lunar and Planetary Science Conference, Houston, TX, Abstract #2052

Pike, R.J. (1974) Ejecta from large craters on the Moon: Comments on the geometric model of McGetchin et al. Earth and Planetary Science, 23, 265-274.

Prettyman, T.H., Hagerty, J.J., Elphic, R.C., Feldman, W.C., Lawrence, D.J., McKinney, G.W., and Vaniman, D.T. (2006) Elemental composition of the lunar surface: Analysis of gamma ray spectroscopy data from Lunar Prospector. Journal of Geophysical Research, 111, E12007, doi:10.1029/2005JR002656.

Ryder, G. and Spudis, P. (1980) Volcanic rocks in the lunar highlands. In Papike, J.J. and Merrill, R.B., Eds., Proceedings of the Conference on the Lunar Highlands Crust, p. 353-375, Pergamon Press.

Ryder, G. and Wood, J.A. (1977) Serenitatis and Imbrium impact melts: Implications for large-scale layering in the lunar crust. Proceedings of the Lunar Science Conference 8th, 655-668.

Sharpton, V.L. (2014) Outcrops on lunar crater rims: Implications for rim construction mechanisms, ejecta volumes, and excavation depths, Journal of Geophysical Research Planets, 119, 154-168, doi: 10.1002/2013JE004523.

Smith, J.V., Anderson, A.T., Newton, R.C., Olsen, E.J., Wyllie, P.J., Crewe, A.V., Isaacson, M.S., and Johnson, D. (1970) Petrologic history of the Moon inferred from petrography, mineralogy, and petrogenesis of Apollo 11 rocks. Proceedings of the Apollo 11 Lunar Science Conference, Pergamon Press, p. 897-925.

Snyder, G.A., Taylor, L.A., and Neal, C.R. (1992) A chemical model for generating the sources of mare basalts: Combined equilibrium and fractional crystallization of the lunar magmasphere. Geochimica et Cosmochimica Acta, 56, 3809-3823, doi: 10.1016/0016-7037(92)90172-F.

Spudis, P.D. (1993) The Geology of Multiringed Basins. 263p, Cambridge University Press, New York.

Stöffler, D., Knoll, H.-D., Marvin, U.B., Simonds, C.H., and Warren, P.H. (1980) Recommended classification and nomenclature of lunar highland rock—A committee report. In J.J. Papike and R.B. Merrill, Eds., Proceedings of the Conference on the Lunar Highland Crust, p 51-70, Pergamon Press

Taylor, G.J., Warren, P. Ryder, G., Delano, J., Pieters, C., and Lofgren, G. (1991) Lunar Rocks. In G.H. Heiken, D. T. Vaniman, and B. M. French, Eds., The Lunar Sourcebook, pp 183-261, Cambridge University Press, Cambridge.

Tompkins, S. and Pieters, C.M. (1999) Mineralogy of the lunar crust: Results from Clementine. Meteoritics and Planetary Science, 34, 25-41.

Warren, P.H. (1985) The magma ocean concept and lunar evolution. Annual Review of Earth and Planetary Sciences, 13, 201-240.

Warren, P.H. (1990) Lunar anorthosites and the magma-ocean plagioclase-flotation hypothesis: Importance of FeO enrichment in the parent magma. American Mineralogist, 75, 46-58.

Warren, P.H. and Wasson, J.T. (1977) Pristine nonmare rocks and the nature of the lunar crust. Proceedings of the 8th Lunar Science Conference, p. 2215-2235.

Wieczorek, M.A. and Phillips, R.J. (1999) Lunar multiring basins and the cratering process. Icarus, 139, 246-259.

Wieczorek et al. (2006) The Constitution and Structure of the Lunar Interior. In Jolliff, B.L., Wieczorek, M.A., Shearer, C.K., and Neal, C.R., Eds., New Views of the Moon, pp221-364, Mineralogical Society of America.

Wieczorek, M.A. et al. (2013) The crust of the Moon as seen by GRAIL. Science, 339, 671-675, doi: 10.1126/science.1231530.

Wood, J.A., Dickey, J.S.J., Marvin, U.B., and Powell, B.N. (1970) Lunar anorthosites and a geophysical model of the moon. Proceedings of the Apollo 11 Lunar Science Conference, pp. 965–988.

Yamamoto, S., Nakamura, R., Ogawa, Y., Ishihara, Y., Morota, T., Hirata, N., Ohtake, M., Hiroi, T., Yokota, Y., and Haruyama, J. (2012) Massive layer of pure anorthosites on the Moon. Geophysical Research Letters, 39, L13201, doi: 10.1029/2012GL052098.

Figure captions

Figure 1. Geometry of the excavation cavity as approximated by Spudis (1993) (not to scale). The excavation cavity diameter is defined by the transient cavity diameter (D_{tc}) taken from Petro and Pieters (2004). The depth of excavation, H_{exc}, is defined by an assumed depth/diameter ratio (R_{dd}) and the transient cavity diameter. The radius of the sphere used to calculate the ejected volume is defined by these parameters. Table 2 shows the transient crater diameters used and the following calculations of total ejected volume and mantle fraction for the 43 lunar basins examined by Petro and Pieters (2004, 2008).

Figure 2. Flowchart describing the procedure used to assign detected minerals to highland rock types for each of the scenarios calculated. A detailed description of the process is located in the accompanying text.

Figure 3. Calculated abundances of a) anorthosite; b) norite; c) troctolite; d) mare basalt; e) dunite; f) pyroxenite; and g) the limiting mafic mineral for all pixels returning no solution as described in Figure 2; for a scenario calculated with purest anorthosites (2 vol% mafic minerals), 2 vol% mantle permitted, and all excess clinopyroxene not assigned to the mantle assigned to mare basalt. The majority of pixels returning no solution were limited by the orthopyroxene required to fulfill our anorthosite mafic composition assumptions in this case. The no-solution pixels were limited to the central farside highlands, an area extremely rich in plagioclase and low in orthpyroxene in the maps of Crites and Lucey (in press). The nearside maria and the areas immediately bordering them, defined as pixels with FeO > 10 wt% as measured by the Lunar Prospector gamma ray spectrometer (2°/pixel maps, Prettyman et al. 2006), are not relevant to this study of the highlands crust and are masked in all maps. 3h) shows the outline of the

masked region overlain on the LRO Wide Angle Camera global mosaic (NASA/GSFC/Arizona State University).

Figure 4. Summary of the range of the relative sources of mafic contaminant consistent with the mineral maps of Crites and Lucey (in press) (dotted field). Open diamonds show scenarios calculated in this work. "Igneous contaminant" includes the highland rock types norite, troctolite, and gabbro, as well as the mare basalt component assumed in some scenarios.

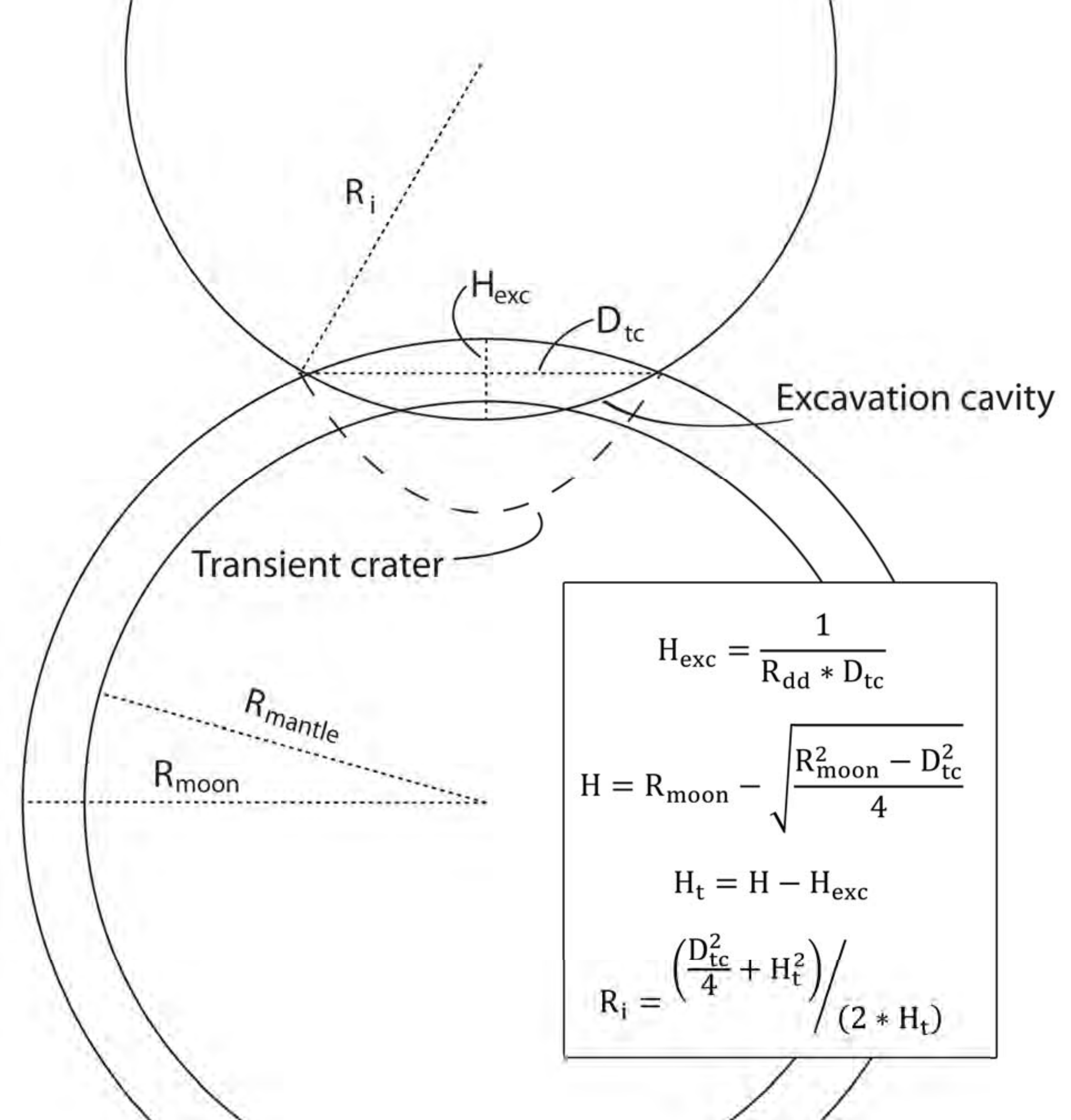

$$H_{exc} = \frac{1}{R_{dd} * D_{tc}}$$

$$H = R_{moon} - \sqrt{\frac{R_{moon}^2 - D_{tc}^2}{4}}$$

$$H_t = H - H_{exc}$$

$$R_i = \left(\frac{D_{tc}^2}{4} + H_t^2\right) \Big/ (2 * H_t)$$

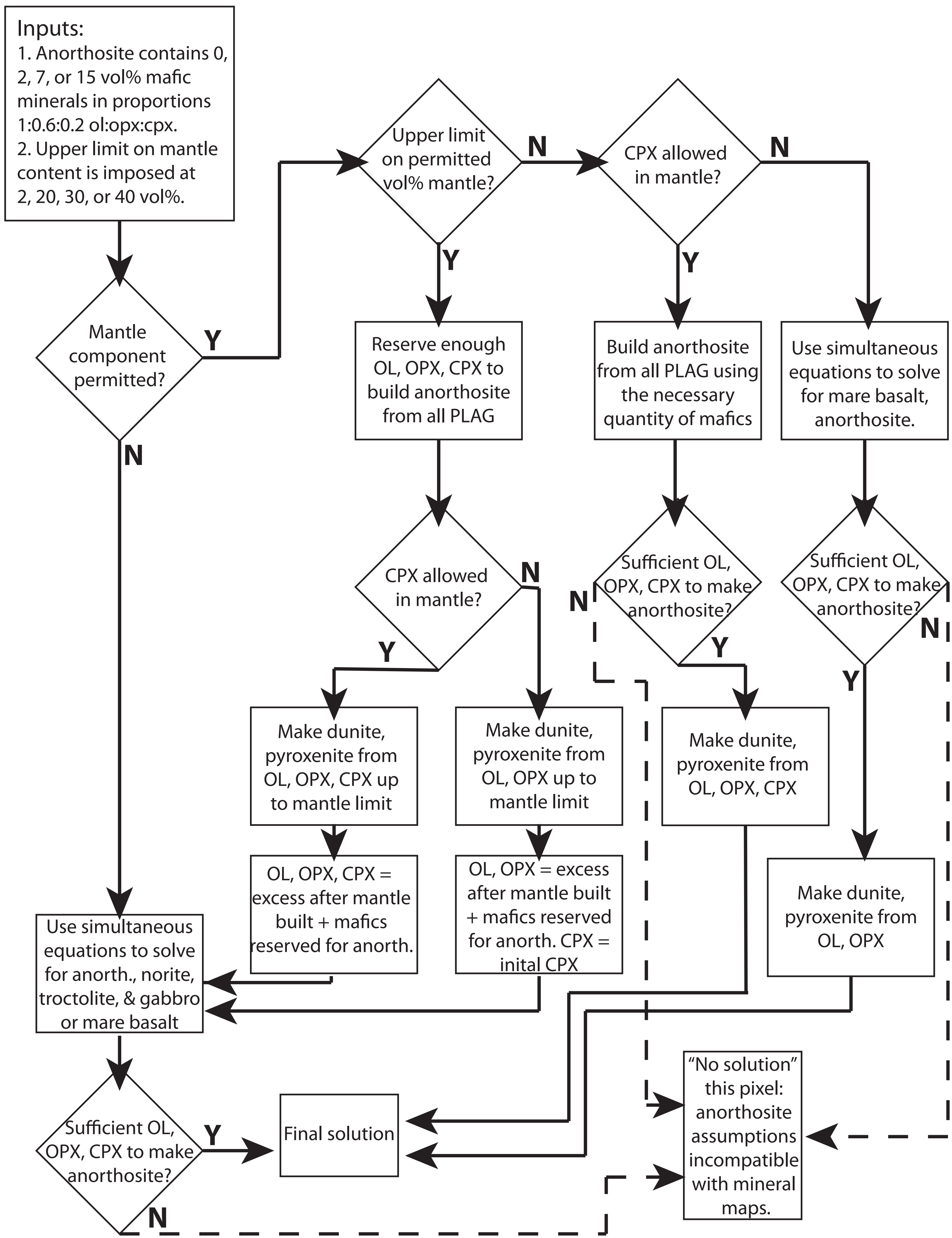

Inputs:
1. Anorthosite contains 0, 2, 7, or 15 vol% mafic minerals in proportions 1:0.6:0.2 ol:opx:cpx.
2. Upper limit on mantle content is imposed at 2, 20, 30, or 40 vol%.
Mantle component permitted?
Y
N
Upper limit on permitted vol% mantle?
N
Y
CPX allowed in mantle?
N
Y
Reserve enough OL, OPX, CPX to build anorthosite from all PLAG
Build anorthosite from all PLAG using the necessary quantity of mafics
Use simultaneous equations to solve for mare basalt, anorthosite.
CPX allowed in mantle?
N
Y
Sufficient OL, OPX, CPX to make anorthosite?
N
Y
Sufficient OL, OPX, CPX to make anorthosite?
N
Y
Make dunite, pyroxenite from OL, OPX, CPX up to mantle limit
Make dunite, pyroxenite from OL, OPX up to mantle limit
Make dunite, pyroxenite from OL, OPX, CPX
Make dunite, pyroxenite from OL, OPX
OL, OPX, CPX = excess after mantle built + mafics reserved for anorth.
OL, OPX = excess after mantle built + mafics reserved for anorth. CPX = inital CPX
Use simultaneous equations to solve for anorth., norite, troctolite, & gabbro or mare basalt
Sufficient OL, OPX, CPX to make anorthosite?
Y
N
Final solution
"No solution" this pixel: anorthosite assumptions incompatible with mineral maps.

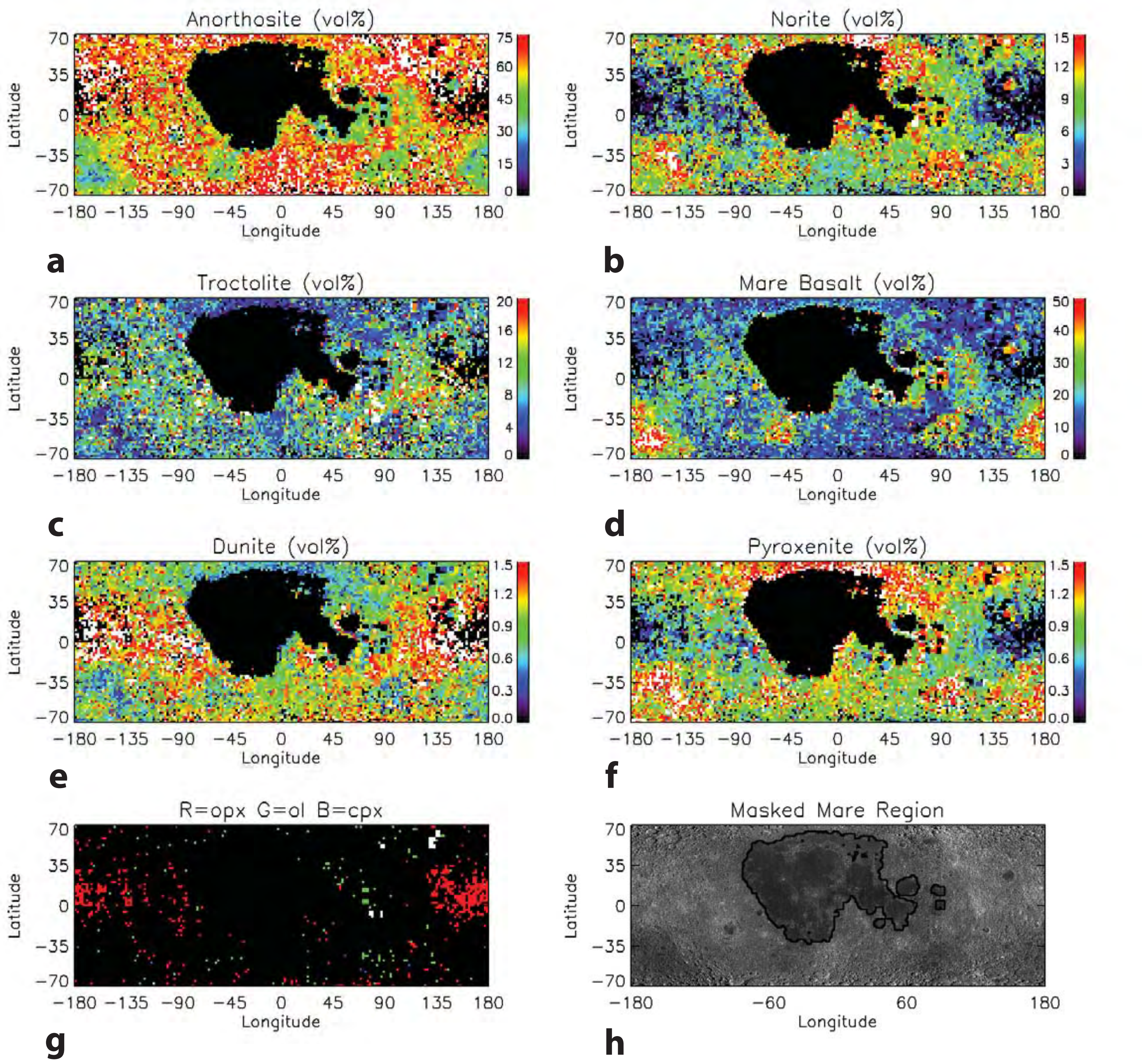
Anorthosite (vol%)
Norite (vol%)
Troctolite (vol%)
Mare Basalt (vol%)
Dunite (vol%)
Pyroxenite (vol%)
R=opx G=ol B=cpx
Masked Mare Region
Latitude
Longitude
70 35 0 −35 −70
−180 −135 −90 −45 0 45 90 135 180
−180 −60 60 180
75 60 45 30 15 0
15 12 9 6 3 0
20 16 12 8 4 0
50 40 30 20 10 0
1.5 1.2 0.9 0.6 0.3 0.0
a
b
c
d
e
f
g
h

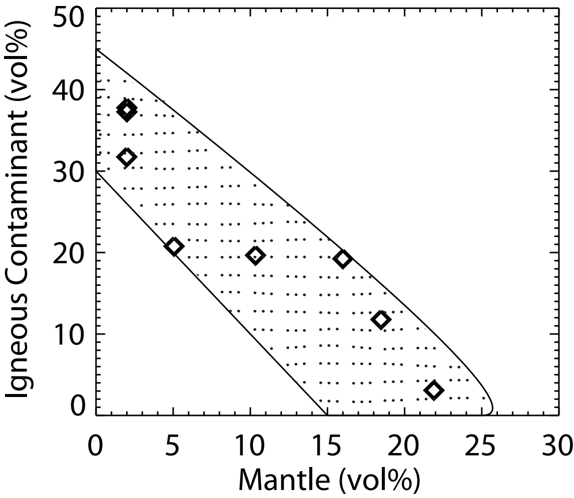

Igneous Contaminant (vol%)
0
10
20
30
40
50
0
5
10
15
20
25
30
Mantle (vol%)

Table 1. Compositions defined for non-endmember rock types.
Notes:
[a]Percent total mafic minerals in anorthosite is varied in our mixing models (0, 2, 7, or 15 vol%)
[b]Based on the composition and rock type interpretation of Mg-suite rocks catalogued by Cahill and Lucey (2007)
[c]Based on compositions of mare basalts from Taylor et al. (1991)
[d]Orthopyroxene and Clinopyroxene go into pyroxenite in the unique proportions in which they are present in each pixel

	% Plagioclase	% Olivine	% Orthopyroxene	% Clinopyroxene
Anorthosite[a]	N	.54*(100-N)	.32*(100-N)	.14*(100-N)
Norite[b]	49	0	51	0
Gabbro[b]	41	0	0	59
Mare basalt[c]	32	0	0	68
Troctolite[b]	53	47	0	0
Dunite	0	100	0	0
Pyroxenite[d]	0	0	OPX + CPX = 100	

Table 2. Sample basin ejecta volume calculations. Transient crater dimensions from Petro and Pieters (2004) for all basins except SPA; SPA transient crater dimensions from Spudis (1993). Depth of excavation = 1/10*TC diameter (Spudis 1993). Ejected volume is calculated following the method of Spudis (1993) as described in text. Crustal thicknesses from Wieczorek et al. (2013).

					Crustal thickness=34 km	Crustal thickness=43 km
Basin	Main ring diameter (km)	Mean transient crater diameter estimation (km)	Depth of excavation (km)	Ejected volume (10^6 km^3)	Mantle volume ejected (10^6 km^3)	Mantle volume ejected (10^6 km^3)
South Pole-Aitken	2600	1470	147	127.01	74	62.44
Tsiolkovsky-Stark	700	409	40.9	2.7	0.08	0
Insularum	600	330	33	1.42	0	0
Marginis	580	315	31.5	1.24	0	0
Flamsteed-Billy	570	307	30.7	1.14	0	0
Balmer	500	252	25.2	0.63	0	0
Werner-Airy	500	252	25.2	0.63	0	0
Pingre-Hausen	300	95	9.5	0.03	0	0
Al-Khwarizmi-King	590	322	32.2	1.13	0	0
Fecunditatis	690	401	40.1	2.55	0.06	0
Australe	880	550	55	6.56	0.95	0.31
Tranquillitatis	700	409	40.9	2.7	0.08	0
Mutus-Vlacq	690	401	40.1	2.55	0.06	0
Nubium	690	401	40.1	2.55	0.06	0
Lomonosov-Fleming	620	346	34.6	1.64	0	0
Ingenii	315	107	10.7	0.05	0	0
Poincare	325	115	11.5	0.06	0	0
Keeler-Heaviside	500	252	25.2	0.63	0	0
Coulomb-Sarton	440	205	20.5	0.34	0	0
Smythii	740	440	44	3.36	0.17	0
Lorentz	365	146	14.6	0.12	0	0
Amundsen-Ganswindt	335	122	12.2	0.07	0	0

Schiller-Zucchius	335	122	12.2	0.07	0	0
Planck	325	115	11.5	0.06	0	0
Birkhoff	325	115	11.5	0.06	0	0
Freundlich-Sharonov	600	330	33	1.42	0	0
Grimaldi	440	205	20.5	0.34	0	0
Apollo	480	236	23.6	0.52	0	0
Nectaris	860	534	53.4	6	0.79	0.23
Mendel-Rydberg	420	189	18.9	0.27	0	0
Moscoviense	420	189	18.9	0.27	0	0
Korolev	440	205	20.5	0.34	0	0
Mendeleev	365	146	14.6	0.12	0	0
Humboldtianum	650	369	36.9	1.98	0.01	0
Humorum	425	193	19.3	0.28	0	0
Crisium	740	440	44	3.36	0.17	0
Serenitatis	920	581	58.1	7.73	1.32	0.52
Hertzsprung	570	307	30.7	1.14	0	0
Sikorsky-Rittenhouse	310	103	10.3	0.04	0	0
Bailly	300	95	9.5	0.03	0	0
Imbrium	1160	769	76.9	17.9	5.53	3.45
Schrodinger	320	111	11.1	0.05	0	0
Orientale	930	589	58.9	8.05	1.43	0.58
TOTAL				209.14	84.71	67.53
Vol% mantle of total ejecta					40.50	32.29
TOTAL scaled to 0.1 km thick ejecta				5.88	2.38	1.90
Vol% mantle of total mixed surface layer					2.09	1.67
TOTAL scaled to 10 km thick ejecta				58.77	23.80	18.98
Vol% mantle of total mixed surface					20.93	16.68

layer							

Table 3. Compositional variable values used in models		
Anorthosite mafic content	0	Extreme case: pure anorthite
	2	Ohtake et al. (2009)
	7	Mean of Wieczorek et al. (2006)
	15	Warren (1990)
Upper limit on mantle component in crust	0	Extreme case: no mantle excavated
	2	Housen et al. (1983) via Petro and Pieters (2008)
	20	Pike (1974) via Petro and Pieters (2008)
	30	Spudis (1993), thick crust
	40	Spudis (1993), thin crust
	No limit	Extreme case: all excess mafics attributed to mantle
Cpx limit in mantle	No limit	CPX permitted in mantle
	0	All CPX due to mare basalt

Table 4. Summary of mixing models most consistent with measured mineralogy of the lunar highlands.

	Description	Mean anorthosite (vol%)	Mean mare basalt (vol%)	Total POI rocks (vol%)	Mantle material (vol%)	Total non-MO rocks (vol%)	% area no solution
Mafics into POI and/or mare basalt	Pure anorthite; all mafics POI	54.87		45.13	0.00	45.13	0.00
	PAN; excess mafics POI	55.69		44.31	0.00	44.31	6.87
	Anorthosites with 7 vol% mafics; excess mafics POI	60.39		39.61	0.00	39.61	18.52
	PAN; excess ol + opx POI; excess cpx mare basalt	58.77	19.43	21.81	0.00	41.23	6.94
Mafics into mantle and/or mare basalt	Pure anorthite; all mafics mantle	75.73		0.00	24.27	24.27	0.00
	PAN; excess mafics mantle	75.50		0.00	23.50	23.50	7.17
Mafics into mantle up to 40%	PAN; mafics to mantle up to 40%; excess ol + opx POI; excess cpx mare basalt	76.54	0.30	0.09	23.07	23.46	51.12
Mafics into mantle up to 30%	PAN; mafics into mantle up to 30%; excess ol + opx POI; excess cpx mare basalt	75.02	2.16	0.92	21.90	24.98	51.71
Mafics into mantle up to 20%	PAN; mafics to mantle up to 20%; excess ol + opx POI, excess cpx mare basalt	69.75	10.33	4.66	18.47	30.25	36.39
	PAN; ol + opx to mantle up to 20%; excess ol + opx into POI; all cpx to mare basalt	69.99	19.39	0.28	10.34	30.01	7.63
Mafics into mantle up to 2%	PAN; mafics to mantle up to 2%; excess ol + opx POI, excess cpx mare basalt	60.22	18.01	19.77	2.00	39.78	7.59
	PAN; ol + opx to mantle up to 2%; excess ol + opx into POI; all cpx to mare basalt	60.73	19.50	17.77	2.00	39.27	8.18